LYAPUNOV-BASED NONLINEAR CONTROL STRATEGIES FOR MANIPULATION OF PARTICLES AND BIOMOLECULES USING OPTICAL TWEEZERS

by

Melika Golgoon

APPROVED BY SUPERVISORY COMMITTEE:

Mark W. Spong, Chair

Alireza Mohammadi

S.O. Reza Moheimani

Waseem Abbas

LYAPUNOV-BASED NONLINEAR CONTROL STRATEGIES FOR MANIPULATION OF PARTICLES AND BIOMOLECULES USING OPTICAL TWEEZERS

by

MELIKA GOLGOON, BS, MS

THESIS

Presented to the Faculty of

The University of Texas at Dallas

in Partial Fulfillment

of the Requirements

for the Degree of

MASTER OF SCIENCE IN

SYSTEMS ENGINEERING AND MANAGEMENT

THE UNIVERSITY OF TEXAS AT DALLAS

December 2024

ACKNOWLEDGMENTS

I am deeply grateful to my advisor, Prof. Mark Spong, whose constant support and understanding have been instrumental in my entire academic journey. Working under his guidance in the Systems Engineering Department at the University of Texas at Dallas has been the most pivotal opportunity of my life, introducing me to the world of control theory and inspiring me to contribute to the field. Prof. Spong has been an exceptional role model; it has been a privilege to learn from his vast expertise and guidance.

I would also like to express my heartfelt appreciation to Prof. Alireza Mohammadi, an outstanding co-advisor and collaborator. He has contributed immeasurably and his expertise, approachability, and meticulous feedback have been invaluable to my research. His insights into control theory, especially its applications in cyber-physical systems, have shaped not only the direction of my research but also deepened my passion for the field. I am also grateful for the support from the National Science Foundation (NSF).

My appreciation extends to Prof. Reza Moheimani and Prof. Waseem Abbas, members of my committee, for their time, insightful feedback, and unwavering encouragement. In addition, the courses they offered significantly contributed to my foundational knowledge in control systems: Prof. Spong in optimization theory and practice, Prof. Moheimani in modeling and simulation, and Prof. Abbas in multi-agent robotics and linear systems. Their collective influence has significantly expanded my understanding of science and engineering, ultimately enabling me to embark on a intriguing career.

The welcoming environment at the Eric Jonsson School, particularly created by staff members like Brenda Rains (Academic Support Coordinator) and Kathryn Grant (Administrative Assistant), made me feel at home as an international student. I am thankful to the Department of Systems Engineering for honoring me with the ECS scholarship. To my colleagues, friends, and office partners, particularly those in the Control Systems Lab, thank you for the inspiring

environment that made this journey enjoyable. While there are too many to name individually, I cherish the company of all the wonderful people I have met at UTD.

Finally, I want to express my sincere gratitude to my family and friends for their unwavering love and support. I am profoundly grateful to my parents, whose efforts ensured I had access to all the opportunities that have brought me to where I am today. My brother, Ashkan, deserves a special mention for his steadfast love, the encouragement throughout the years, and the motivation he brings to every step of my journey. I could not have reached this milestone without each of you.

November 2024

LYAPUNOV-BASED NONLINEAR CONTROL STRATEGIES FOR MANIPULATION OF PARTICLES AND BIOMOLECULES USING OPTICAL TWEEZERS

Melika Golgoon, MS
The University of Texas at Dallas, 2024

Supervising Professor: Mark W. Spong, Chair

Tweezers-based nanorobots, optical tweezers in particular, are renowned for their exceptional precision, and among their biomedical applications are cellular manipulation, unzipping DNAs, and elongating polypeptide chains. This thesis introduces a series of Lyapunov-based feedback control frameworks that address both stability and controlled instability for biological manipulation, applied within the context of optical tweezers. At the core of this work are novel controllers that stabilize or destabilize specific molecular configurations, enabling fine manipulation of particles like polystyrene beads and tethered polymers under focused laser beams.

Chapter §1 covers the foundational principles and surveys existing literature on the modeling and control of optical tweezers, emphasizing gaps in the stability and instability control of molecular systems. Chapter §2 presents a robust Control Lyapunov Function (CLF) approach, designed to stabilize spherical particles under optical trapping. By formulating a smooth, norm-bounded feedback controller, we achieve lateral stabilization despite external disturbances, using a real-time, static nonlinear programming (NLP) solution. Simulations verify the effectiveness of this CLF framework, even with significant initial displacements from the laser focus and under thermal forces modeled as a white Gaussian noise.

Chapter §3 addresses controlled instability through a Control Chetaev Function (CCF) framework, specifically targeting protein unfolding applications. Linearization with respect to the control input facilitates the application of destabilizing universal controls for affine-in-control system dynamics. The resulting CCF-based norm-bounded feedback controller induces system instability by laterally extending the trapped DNA handle, thereby increasing the molecular extension and providing insights into protein denaturation and unfolding pathways. This controller is robust to stochastic thermal forces and optimized for real-time computational efficiency.

These Lyapunov and Chetaev-based control designs collectively expand the capabilities of optical tweezers, advancing single-molecule manipulation under both stable and unstable conditions. These findings advance precision nanomanipulation, opening new avenues for exploring the molecular mechanics of protein unfolding and DNA elasticity.

TABLE OF CONTENTS

LIST OF FIGURES

LIST OF TABLES

CHAPTER 1

INTRODUCTION

The introduction outlines the main biological applications of robotic nanomanipulation §1.1 as well as historical background and fundamentals of optical tweezers §1.2. Discussing the fundamentals, we next proceed to cover some prior literature on modeling efforts for polymer elasticity §1.3, current understanding of optical tweezers in single-molecule studies, and the advanced control systems used to enhance their capabilities §1.4. Finally, we highlight the existing gaps in the current literature §1.5, contributions of our work, and organization of the thesis §1.6.

1.1 Biological Applications of Robotic Nanomanipulation

Closed-loop control algorithms facilitate precise automated and semi-automated operations at micro- and nanoscale levels (Oubellil et al., 2019). Thanks to substantial advances in chemistry, physics, and nanotechnology, significant accomplishments in nanorobotic devices have been achieved. Nanorobotic devices are either tiny themselves (nanorobots) or target minute particles (nanomanipulators). They both complement each other and play a crucial role in developing medical robotics as well as advancing the treatment and diagnosis of diseases, especially in the field of personalized precision medicine (Zarrintaj et al., 2022). Robotic nanomanipulation, which includes tweezers-based nanomanipulators (Grier, 2003; Ashkin et al., 1986), AFM-based nanomanipulators (Li et al., 2023; Lal and John, 1994; Xie and Régnier, 2010; Onal et al., 2010), and EM-based nanomanipulators (Shi et al., 2016), has to do with capturing and moving nano-objects, within the range of tens of nanometers to tens of microns. Therefore, robotic nanomanipulation enables effective interaction with such biological entities with the same range size as biomolecules, organelles, cells, and most proteins. Accordingly, biomedical nanomanipulation brings great awareness to the molecular

mechanisms, the interaction between drug molecules and diseased cell molecules, as well as pathological changes in cells. Hence, robotic nanomanipulators are widely utilized in genetic disease therapy such as cancer and biomedicine applications, including cellular manipulation, abrupt withdrawal, and targeted drug delivery. We refer the reader to (Li et al., 2020) for a comprehensive survey on biomedical applications of nanorobotics. Next, we discuss the fundamental background of optical tweezers.

1.2 Historical Background and Fundamentals of Optical Tweezers

Optical tweezers are known as powerful tools for manipulating individual molecules and studying their properties at the nanoscale. They remotely probe biological samples by precisely holding and manipulating the nano-object of interest in a focal point of a highly focused laser beam as their end-effector. In the late 80s, Ashkin (1980) in a seminal work utilized optical tweezers to levitate dielectric particles and single atoms (see Figure 1.1 for its principle of operation). According to Ashkin (1980), trapping forces arise from the laser radiation forces symmetrically crossing the particle, conserving the net momentum of zero, and preventing its horizontal movements. Moreover, according to Maxwell, the momentum of laser light is small and is canceled out with the gravity applied in the opposite direction, and thus, keeping the particle from deviating in the vertical direction. Therefore, it is concluded that one can optically view and levitate a particle by directing a Gaussian laser beam vertically across it and that the particle's stability and dynamics of motion solely depend on applied horizontal forces. Since then, optical tweezers have been widely used in biological applications, including the study of molecular motors, DNA mechanics, and protein/RNA folding/unfolding (Bustamante et al., 2021; Kellermayer et al., 1997; Bustamante et al., 2020). In the last one, the first and last amino acids of the chain, N- and C-termini, respectively, are typically tethered between two optically trapped beads or between a bead and a surface (i.e., AFM cantilever), allowing the protein to get mechanically unfolded through the movement of

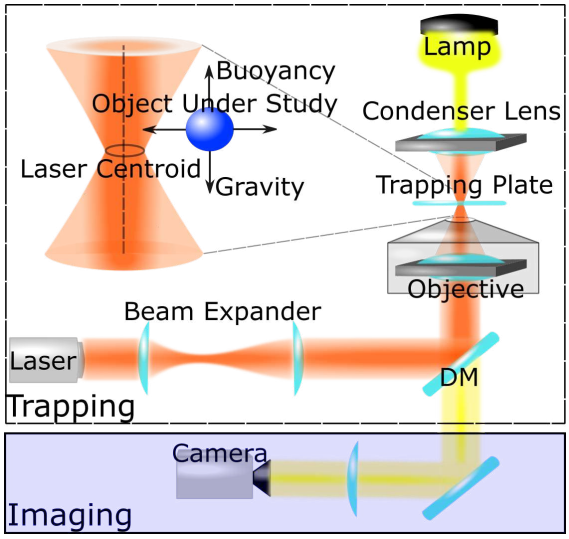

Figure 1.1: Schematic of a typical optical tweezer system. The imaging setup consists of a charge-coupled device (CCD) camera, which is able to monitor and track the cell's change of position in real-time. The main feature is the trapping setup, in which the laser beam is magnified using a beam expander, directed onto a dichroic mirror, and then transmitted to a motorized oil-immersion objective. The objective involves a lens with a high numerical aperture that centralizes the beam to the wavelength of interest and traps the immersed cell in the medium and on the trapping plane.

the device (Bustamante et al., 2020). Moving the optical tweezers device and recording the response of the chain to mechanical denaturation provide valuable information on protein folding thermodynamics and kinetics that is challenging to attain through traditional ensemble methods (Neuman and Nagy, 2008; Bustamante et al., 2020).

1.3 Modeling Polymer Elasticity

Accurate modeling of polymer elasticity is crucial for interpreting optical tweezers measurements. The foundation to the worm-like chain (WLC) model, introduced by Kratky and Porod (1949), has become the standard framework for describing the elastic properties of semiflexible biopolymers like DNA under applied force. Unlike simpler models like the freely-jointed chain (FJC), the WLC model describes the bending rigidity of the polymer backbone and provides a more accurate representation of force-extension behavior, especially

in the low and intermediate force regimes relevant to many single-molecule experiments. The WLC model has been successfully applied to model the elasticity of DNAs commonly used in optical tweezers protein folding studies. Bustamante et al. (2020) provided an influential early demonstration of WLC behavior in single DNA molecules stretched with optical tweezers. Subsequent work has refined the WLC model to account for phenomena like enthalpic stretching at high forces, which becomes significant when the applied force approaches or exceeds tens of piconewtons (Andersen and Chen, 2024; Fiasconaro and Falo, 2023). Stigler et al. (2011) used WLC model to analyze the complex folding pathway of calmodulin, enabling precise measurement of the length of the polypeptide chain in the unfolded state at a subnanometer scale and identifying several on- and off-pathway intermediates. Hyeon and Thirumalai (2006) developed a more sophisticated model that accounts for the heterogeneous flexibility of unfolded proteins. Pfitzner et al. (2013) characterized the mechanical properties of DNA origami beams, showing their effectiveness as extremely rigid handles for precise, high-resolution measurements.

In protein folding/unfolding studies, it is often necessary to model both the unfolded/folded polypeptide and its trapping handle. (Ranaweera et al., 2003) introduced fundamental control techniques for stabilizing spherical particles in optical tweezers. (Ranaweera et al., 2004) further refined the model by analyzing lateral escape times under thermal noise. (Ranaweera and Bamieh, 2005) explored advanced control schemes, improving stability against position fluctuations. Later, (Li et al., 2013) applied closed-loop control to ensure robust trapping of biological cells, while (Li and Cheah, 2017) addressed stochastic disturbances, using adaptive neural networks to enhance trapping stability. Following that, (Zhang et al., 2019) expanded the manipulation capabilities to 3D environments using magnetic tweezers, enabling versatile control in complex settings. Finally, (Golgoon et al., 2024) proposed a control Lyapunov function (CLF) framework for closed-loop control design of polystyrene beads, commonly used as manipulating handles in optical tweezers experiments, further advancing force calibration accuracy.

1.4 Optical Tweezers for Single-Molecule Studies

Key capabilities of optical tweezers include the ability to apply precisely controlled forces, measure molecular extensions with sub-nanometer accuracy, and observe rare folding events and transient intermediates that are obscured in bulk experiments (see, e.g., (Bustamante et al., 2004) and (Zaltron et al., 2020) for a comprehensive review of protein (un)folding studies using optical tweezers). The high resolution of optical tweezers has enabled detailed mapping of protein folding energy landscapes. Neupane et al. (2016) used an ultrastable optical trap to directly observe the transition path time during protein folding, providing experimental validation of theoretical models of barrier crossing dynamics. Yu et al. (2012) applied a similar approach to analyze misfolding pathways in prion proteins, uncovering greater landscape roughness associated with pathological aggregation. Jahn et al. (2016) utilized optical tweezers to study the folding pathway of the molecular chaperone (Hsp90), uncovering a tendency for rapid domain misfolding that is mitigated by mechanical tension, highlighting how single-molecule manipulation reveals folding mechanisms crucial to cellular protein quality control.

Tweezers Control Strategies. Precise control over applied forces is critical for many optical tweezers applications (Greenleaf et al., 2005), namely: i) *Optical Force-Clamp Systems.* Traditional optical force-clamp systems often rely on active feedback mechanisms such as proportional-integral-derivative (PID) controllers to a maintain constant force or position. These systems are constrained by thermal fluctuations and the flexibility of the molecules involved, which can affect the precision of force application (see, (Bugiel et al., 2017)). Advanced control strategies such as the mixed objective $H2 - H\infty$ optimization framework, have been developed to tackle the challenges of force control and real-time motion tracking, these methods offer measurable assurances for force regulation while reducing errors in step estimation, achieving high precision in force application. Plus, the ability to maintain constant

forces over long durations enables detailed analysis of motor protein behavior under different load conditions (see, (Roychowdhury et al., 2013) and (Roychowdhury et al., 2013)). ii) *Acousto-Optic Deflectors.* The use of acousto-optic deflectors allows for rapid adjustments to the trapping beam position. This capability is crucial for studying dynamic processes such as molecular unfolding, where force stability is essential (Mack et al., 2009). The integration of real-time step detection schemes allows for the extraction of stepping data in the presence of thermal noise, enhancing the accuracy of molecular motion studies. The detection of step-like features in noisy data is essential for analyzing single-molecule dynamics, particularly where thermal noise is a significant factor (see, (Loeff et al., 2021; Tyson et al., 2015)).

Precise Manipulation and Control Algorithms. The precise manipulation of optically targeted molecules relies on designing real-time, robust control algorithms to locate and move the micro/nano-object of interest (e.g., see (Ranaweera et al., 2003, 2004; Ranaweera and Bamieh, 2005; Li et al., 2013; Li and Cheah, 2017; Zhang et al., 2019, 2020; Mohammadi and Spong, 2022a)). This purpose is subjected to some challenges, especially when the design of closed-loop feedback controllers is discussed, including trapping failure when particles drift from the laser beam, trap Brownian motion due to thermal noise fluctuations, unknown spatially varying stiffness, and the computational complexity of implementing effective control algorithms.

The Control Lyapunov Function (CLF) framework offers formal guarantees for stability, while also being able to manage unmodeled dynamics and parametric uncertainties. Therefore, CLF-based frameworks beyond their widespread use in robotics and autonomous systems (e.g., (Galloway et al., 2015; Taylor et al., 2019; Kubo et al., 2020)) are a promising tool for designing closed-loop control algorithms in nanomanipulation tasks via optical-tweezers. A major challenge, especially for non-affine-in-control systems, is constructing suitable CLFs, often requiring computationally intensive methods like sum-of-squares (SOS) programming (Furqon et al., 2016) or Zubov's method (Camilli et al., 2008).

1.5 Gaps in the Existing Literature

In the realm of nanopositioning, Li et al. (2021) utilized integral resonant control (IRC) to adjust resonant frequencies, significantly increasing closed-loop bandwidth and reducing tracking errors in piezo-actuated nanopositioners. Hong et al. (2020) further enhanced these results by combining IRC with input shaping, achieving bandwidth improvements up to eight times over standard PI control. Yang and Youcef-Toumi (2022) proposed a decoupled tracking and damping control strategy using multimode charge sensing, simplifying the control design while offering wide bandwidth and enhanced stability, effectively addressing challenges such as hysteresis and mechanical resonances. Mohammadi and Spong (2022b) uses a quadratic optimization-based nonlinear control approach to guide protein folding by minimizing deviations from a reference vector field, ensuring stable conformation prediction while avoiding high-entropy-loss routes. Similarly, several closed-loop control algorithms have been proposed for optical tweezer-based nanomanipulation, including a globally asymptotically stabilizing (GAS) control law based on saturation analysis (Ranaweera et al., 2003; Ranaweera and Bamieh, 2005), a sliding mode control scheme with adaptive observers (Li et al., 2013), a controller utilizing adaptive neural networks (Li and Cheah, 2017), a visual servo proportional control law (Zhang et al., 2019, 2020), and a Chetaev control framework for protein unfolding (Mohammadi and Spong, 2022a). Despite the rise of optimization-based nonlinear controllers, such as MPC-based controllers (see, e.g., (Chi et al., 2022)), optimal decision strategy (ODS)-based frameworks (see, e.g., (Mohammadi and Spong, 2021, 2022b)), and CLF-based schemes (e.g., (Reed et al., 2023)), which inherently address stability and safety concerns, a similar framework is still lacking for optical tweezers. While much work with optical tweezers has focused on studying stable protein conformations, inducing and characterizing unstable states presents unique challenges. Traditional approaches aim to stabilize systems, yet deliberately introducing controlled instability requires a different framework.

Exploring control schemes in optical tweezers to induce non-equilibrium behavior is a novel research area. Current research primarily focuses on stability and constant forces, with limited attention to controlled instability (da Fonseca et al., 2024). Challenges in controlling nanoparticles for spectroscopy and microscopy have underscored the need for advanced control schemes to manage instability in a controlled manner (Chen et al., 2022). Exploring these advancements could lead to significant breakthroughs in manipulating non-equilibrium behaviors in optical tweezers systems.

The Chetaev instability theorem provides a rigorous mathematical basis for inducing instability and analyzing unstable equilibria in nonlinear dynamical systems (Braun et al., 2018). In the broader field of stochastic control, there has been growing interest in controllers that shape non-equilibrium distributions rather than simply stabilizing equilibrium. A recent study by (Zhao et al., 2022) proposed a novel control system using a self-organizing fuzzy cerebellar neural network model designed for the accurate manipulation of biological cells using holographic optical tweezers, showcasing advanced control strategies for non-equilibrium systems at the microscopic scale. (Mohammadi and Spong, 2022a) applied Chetaev functions within a kinetostatic compliance framework to develop destabilizing control inputs that systematically elongate protein molecules, highlighting the theorem's potential for controlled protein unfolding. (Efimov et al., 2014) extended this approach to develop necessary and sufficient conditions for instability in terms of Chetaev functions, thereby opening up new possibilities for manipulating molecular systems in a controlled, unstable state. Applying Chetaev-based control to the nonlinear and stochastic dynamics of optically trapped biomolecules represents a novel and potentially powerful approach that has not been previously explored.

1.6 Contributions and Organization of the Thesis

This thesis seeks to tackle the issue of stability and instability of equilibria through a proper design of Lyapunov-based feedback controllers, enabling robust manipulation of biological entities via optical tweezers.

Chapter 2 proposes necessary and sufficient conditions for constructing smooth CLFs, along with conditions on the trap stiffness. In particular, it addresses system stability through optimization-based (static nonlinear programming problem along with a one-dimensional search), closed-loop feedback control design, and with the utilization of Control Lyapunov Functions (CLFs). Next, simulation results confirm the effectiveness of the CLF-based control algorithms compared to a well-known GAS control law in the optical tweezers control literature (Ranaweera et al., 2003; Ranaweera and Bamieh, 2005).

Chapter 3 discusses several gaps that were mentioned above. We develop a novel Control Chetaev Function (CCF) framework for inducing controlled instability in an optical tweezers system. This represents the first application of Chetaev-based control to single-molecule manipulation, bridging a significant gap in the literature. Our approach explicitly incorporates the nonlinear WLC model of DNA elasticity into the control system design. We demonstrate how the CCF framework can be used to design controllers that extend tethered DNA molecules in a controlled manner, providing a new tool for probing non-equilibrium polymer dynamics. This is particularly important for studying transient states and folding intermediates that are inaccessible through traditional stabilization-focused control methods. Our stochastic simulations incorporate thermal fluctuations via the overdamped Langevin equation, validating the robustness of the control scheme to Brownian motion, stiffness change, and the rate of collapse of the chain. By combining rigorous nonlinear control theory with polymer physics models, this work aims to enhance the functionality of optical tweezers for accurate handling of single molecules under non-equilibrium conditions. The CCF approach developed could potentially be adapted to a broad spectrum of applications for optical tweezers in biophysics

and nanotechnology, opening new avenues for the study of dynamic molecular processes that require precise, controlled instability.

Ultimately, numerical simulations at the end of Chapters 2 and 3 showcase the reliability and efficiency of the proposed control framework, even under position fluctuations induced by thermal noise. Finally, Chapter 4 provides a comprehensive summary of the findings and key conclusions drawn from this study.

Notation. Given an integer m and a vector $\mathbf{x} \in \mathbb{R}^m$, we let $|\mathbf{x}| := \sqrt{\mathbf{x}^\top \mathbf{x}}$. This denotes the Euclidean norm, and $\|u\|$ indicates the supremum of a function $u(\cdot)$.

CHAPTER 2

CONTROL LYAPUNOV FUNCTION (CLF) FRAMEWORK FOR PARTICLE NANOMANIPULATION

2.1 Introduction

This chapter develops a Control Lyapunov Function (CLF)-based framework to stabilize spherical particles in optical tweezers, addressing the challenges of precise positioning and thermal management. We begin by presenting the force field model and trap dynamics 2.2, drawing on the control-oriented model by Bamieh and colleagues. Key forces, including thermal fluctuations and viscous drag, are also incorporated to capture realistic particle behavior. We, then, detail the trap characteristics and optical tweezer control system resulting, in a non-affine-in-control model that forms the basis for the control design.

In the control problem formulation 2.4, we set the objective of robustly stabilizing the particle at the trap center, accounting for thermal disturbances and measurement errors. Next, we introduce the CLF-based closed-loop control algorithm 2.5, deriving smooth CLFs with conditions that guide stabilizing feedback control. Moving forward to Simulation studies 2.5.3, we demonstrate the effectiveness of the CLF-based control.

By constraining trap stiffness, the control model reduces power fluctuations, protecting sensitive biomolecules from excessive heating. In summary, this CLF-based framework enhances control capabilities at the nanoscale, setting the groundwork for manipulating biomolecules such as DNA, RNA, and proteins—a topic we explored in Chapter 3.

2.2 Force Field Model and Trap Dynamics

In this study, we employ the control-focused model developed by Bamieh and colleagues (see, (Ranaweera et al., 2003; Ranaweera and Bamieh, 2005)). They capture the behavior of small beads suspended in a solvent (such as water or glycerol) by modeling the optical

tweezer force as a nonlinear spring force acting on the beads. This approach is consistent with experimental observations reported by Simmons *et al.* (Simmons et al., 1996). The parameters for the optical tweezers used in this model are provided in Table 2.1 and are taken from (Ranaweera et al., 2003; Ranaweera and Bamieh, 2005). Additionally, based on existing nanomanipulation literature (see, e.g., (Zhang et al., 2020, 2019)), we assume that the gravitational and buoyant forces effectively cancel each other out.

Table 2.1: Optical Tweezers simulation parameters.

Variable	**Value**	**Variable**	**Value**
m	5.5×10^{-10} mg	r_p	1 μm
α_3	22 pN/μm^3	α_1	10 pN/μm
R	0.674 μm	$R_{\max}$	0.3893 μm

The Trapped Particle Equation of Motion. The governing equation of motion for a trapped bead of mass m subject to the optical trapping force $F_t(\cdot)$, viscous drag force $F_d(\cdot)$, and external disturbances $F_e(\cdot)$, arising from factors like thermal noise, is expressed as

$$m\ddot{x} = F_t(x_r) + F_d(\dot{x}) + F_e(t), \tag{2.1}$$

where the relative position of the bead (x_r) is defined based on the lateral position of the bead (x) and the laser focus position (x_T) as follows

$$x_r := x - x_T. \tag{2.2}$$

In Equation (2.1), the nonlinear trapping force is given by

$$F_t(x_r) = \varphi(x_r)\big(\alpha_3 x_r^3 - \alpha_1 x_r\big), \tag{2.3}$$

with a saturation condition as follows

$$\varphi(y) := \begin{cases} 1 & \text{for } |y| < R \\ 0 & \text{otherwise.} \end{cases} \tag{2.4}$$

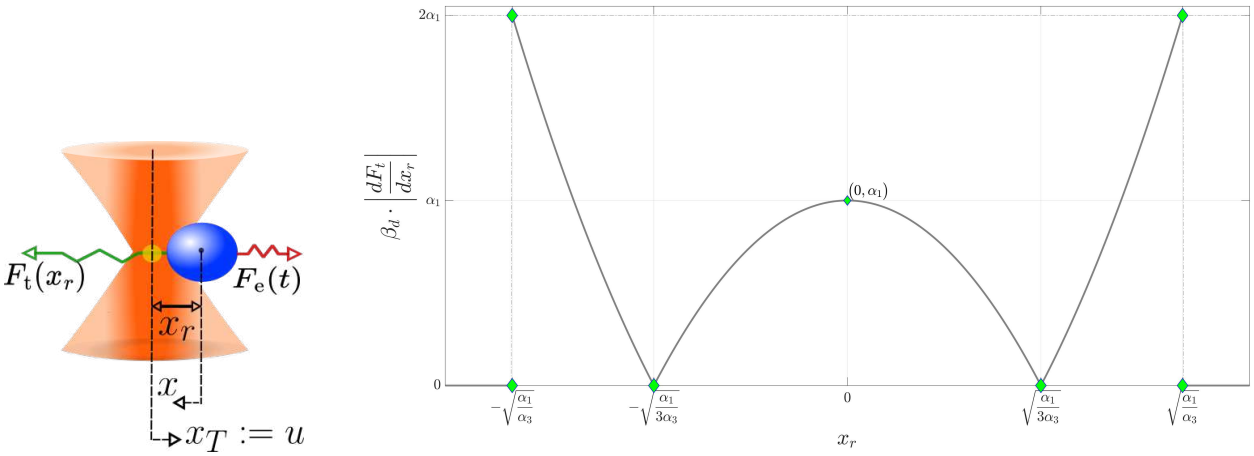

Figure 2.1: The optical tweezer control scheme and its stiffness: The right figure depicts the profile of $\beta_d \cdot |\frac{dF_t}{dx_r}|$ versus x_r; the left one demonstrates the key variables in the optical tweezer non-affine-in-control system model, clearly depicting the bead under the force profile. Thermal fluctuations tend to displace the particle from the trap, while the trapping force pulls it back toward the laser focus, maintaining a state of dynamic equilibrium.

Finally, the viscous drag force $F_d(\cdot)$ reads as

$$F_d(\dot{x}) = -\beta_d \dot{x}, \tag{2.5}$$

where the viscous damping coefficient for a bead with radius r_p suspended in a fluid with viscosity η_f can be calculated using Stoke's equation as $\beta_d = 6\pi\eta_f r_p$.

The Optical Tweezer Control System. The interplay between inertia and viscous drag dictates the dynamic behavior of particles trapped by the optical tweezer. Owing to the inherent scaling laws governing these forces, microscopic particles confined within a harmonic potential and subjected to low Reynolds number conditions (characterized by slow motion within a viscous medium) experience a predominant influence of viscous drag on their inertial motion (see, e.g., (Bustamante et al., 2020) for further details). Consequently, assuming a low Reynolds number regime, where viscous forces prevail over inertia, one can neglect the inertial effects and arrive at the following non-affine-in-control control system

$$\dot{x} = f_{\text{twz}}(x, u, F_e),\ x \in \mathbb{R},\ u \in \mathcal{U},\ F_e \in \mathcal{D}, \tag{2.6}$$

where $f_{\text{twz}} : \mathbb{R} \times \mathcal{U} \times \mathcal{D} \to \mathbb{R}$ is the continuous function

$$f_{\text{twz}}(x, u, F_e) := \frac{\varphi(x-u)}{\beta_d}[\alpha_3(x-u)^3 - \alpha_1(x-u)] + \frac{F_e}{\beta_d}, \tag{2.7}$$

and $\mathcal{U} \subset \mathbb{R}$, $\mathcal{D} \subset \mathbb{R}$ are some closed intervals, respectively. Furthermore, the control input u is the laser focus position, namely, $u := x_T$. In (2.6), the control input can be any measurable locally essentially bounded signal $u(\cdot) : [0, \infty) \to \mathcal{U}$ and the disturbance $F_e(\cdot) : [0, \infty) \to \mathcal{D}$ is assumed to be locally essentially bounded and Lebesgue measurable. Finally, the continuity of $f_{\text{twz}}(\cdot)$ implies that the trapping radius R in (2.4) should satisfy $R = \left(\frac{\alpha_1}{\alpha_3}\right)^{0.5}$. The left schematic diagram in Figure 2.1 demonstrates the important variables of the model given by (2.6).

2.3 Trap Characteristics.

The optical trap is characterized by several key parameters that define its ability to hold and manipulate particles. Among these parameters are the range of influence, maximum force strength, trap stiffness, and capture range velocity (see (Ranaweera, 2004)).

i) *Range of Influence.* The influence range R refers to the maximum distance at which a particle can still feel the restoring force of the trap. Beyond R, the particle is no longer pulled toward the trap center. The lateral influence range can be experimentally determined by observing the distance at which particles are no longer affected by the trap. $R = \sqrt{\frac{\alpha 1}{\alpha 3}}$ is approximately equal to $0.675\mu m$ for a $1\mu m$ spherical bead, and its influence is posed as a saturation function in (2.4).

ii) *Strength (Maximum Force).* The maximum force, $(F_t)_{\max}$, denotes the peak restoring force exerted by the trap. For the spherical particle under study, $(F_t)_{\max}$ and the corresponding maximum range of force, $R_F = \sqrt{\frac{\alpha 1}{3\alpha 3}}$, are approximately 2.60 pN and 0.389 μm respectively.

These values can vary depending on particle size, the configuration of the trap, and laser power (see (Ranaweera and Bamieh, 2005; Nieminen et al., 2007)).

iii) *Trap Stiffness.* The trap stiffness is defined as $\kappa(x) = \frac{dF_t}{dx}$ (where $\frac{dF_t}{dx} = \frac{dF_t}{dx_r}$ by the chain rule), with $F_t(x)$ representing the trap force as given in (2.3). Therefore, it follows that

$$\left|\frac{dF_t}{dx_r}\right| = \left|\frac{\delta(x_r)}{\beta_d}\left\{3\alpha_3 x_r^2 - \alpha_1\right\}\right|. \tag{2.8}$$

It is the measure of the force required to displace a trapped particle from the center of the trap, and higher stiffness implies that the particle is more tightly confined, making it more resistant to thermal fluctuations. It depends on aspects such as refractive index of the immersed medium, laser wavelength and power, as well as particle characteristics like size, shape, and refractive index (Ranaweera, 2004). The plot on the right in Figure 2.1 illustrates the relationship between $\beta_d \cdot \left|\frac{dF_t}{dx_r}\right|$ and the relative position of the bead, denoted as x_r. At $x_r = 0$, the trap stiffness matches the Hookean constant of the optical tweezer, given by $\frac{\alpha_1}{\beta_d}$. In contrast, for larger displacements within the laser half-width the behavior is analogous to a nonlinear restoring spring (see, i.e., (Ghislain et al., 1994; Lee and Padgett, 2012; Jones et al., 2015)).

iii) *Trap Effective Stiffness.* α_e reflects the trap's strength in real, often noisy environments, accounting for factors like thermal fluctuations, trap nonlinearities, and external forces. These environmental influences make effective stiffness lower than ideal stiffness. Inside the limits of the linear force range (R_l), $\alpha_e \approx \alpha_1$, outside this range, as $|x_r|$ increases beyond R_l, the system enters a nonlinear force regime where $\alpha_1 > \alpha_e(x_r) > 0$, and eventually reaches zero when the particle is beyond the trap's range of influence R. While increasing laser power raises this stiffness and strengthens the trap, excessive power can lead to sample heating, risking biological damage in a phenomenon called "opticution." Therefore, managing effective stiffness in real conditions is essential. In 2.5.3, we capture the controller's performance

in managing effective stiffness, including thermal noise, to mimic real-time experimental conditions closely.

iv) *Capture Range Velocity.* The capture range velocity, denoted by v_R, represents the maximum speed at which moving particles can be decelerated and trapped by the optical tweezers. It is the speed threshold at which over half of particles entering the trap's range of influence are captured.

v) *Trap Strength Factors.* Trap strength is influenced by various laser parameters, including power, wavelength, and numerical aperture, which collectively determine the laser's intensity gradient and focus. Increasing the laser power and reducing the focus size enhances the trap's ability to stably hold particles. Polarization also impacts lateral trapping forces, with forces parallel to the light's polarization state being slightly stronger than those perpendicular.

vi) *Particle Properties.* Trapping efficiency also varies based on the size of the trapped particle, shape, and refractive index. For particles roughly equal to the laser wavelength, trapping is optimal, as these particles respond effectively to the intensity gradients generated by the optical tweezers.

The Optical Tweezer Toolbox generates synthetic experimental data and force profiles with varying trap characteristics, including particle properties, beam type, and trap stiffness, allowing detailed simulation and analysis of trapped particle behavior under different conditions (see (Nieminen et al., 2007)).

2.4 Control Problem Formulation and Objective

For the non-affine-in-control optical tweezer system described in (2.6), our goal is to robustly stabilize the position of the bead x at the origin using a feedback input $u = k(x)$ that ensures robust stability, accounting for measurement errors $e(\cdot)$ and external disturbances $F_e(\cdot)$. In particular, we consider the dynamics

$$\dot{x}(t) = f_{\text{twz}}\Big(x(t),\, k\big(x(t)+e(t)\big),\, F_e(t)\Big). \tag{2.9}$$

This refers to the control system in (2.6) governed by the state feedback control law $u = k(x)$, with sensor measurement error $e(t)$ and external disturbances $F_e(t)$. Our aim is to determine a robustly stabilizing feedback, following the approach of Ledyaev and Sontag (Sontag, 2009; Ledyaev and Sontag, 1999), that remains robust against measurement errors $e(\cdot)$ and external disturbances $F_e(\cdot)$, driving the states of the perturbed system (2.9) into a small neighborhood around the origin.

2.5 CLF-Based Closed-Loop Control Algorithm

In this section, we present our solution to the control problem outlined in Section 2.4, employing smooth Control Lyapunov Functions (CLFs) and CLF-based robustly stabilizing feedback control methods developed by Ledyaev and Sontag (see, e.g., (Sontag, 2009; Ledyaev and Sontag, 1999)). We first establish the necessary and sufficient conditions for smooth CLFs in the context of optical tweezers in Section 2.5.1, followed by our CLF-based control algorithm in Section 2.5.2.

2.5.1 Construction of Smooth CLFs for the Optical Tweezer Control System

Consider the non-affine-in-control nonlinear system (2.6) without disturbances, i.e., $F_e = 0$. A differentiable function $V : \mathbb{R} \to \mathbb{R}_{\geq 0}$ qualifies as a smooth *control Lyapunov function (CLF)* for the *unperturbed* optical tweezer system (2.6), with $F_e = 0$, if $V(\cdot)$ is positive definite, proper, and infinitesimally decreasing. It indicates the existence of a positive definite continuous function $W : \mathbb{R} \to \mathbb{R}_{\geq 0}$ and a nondecreasing function $\sigma : \mathbb{R}_{\geq 0} \to \mathbb{R}_{\geq 0}$ such that

$$\sup_{x\in\mathbb{R}} \min_{|u|\leq\sigma\left(|x|\right)} \nabla V(x) \cdot f_{\text{twz}}(x,\, u,\, 0) + W(x) \leq 0. \tag{2.10}$$

Remark 1. *The constraint* $|u| \leq \sigma\big(|x|\big)$ *in the definition of differentiable CLFs theoretically prevents unbounded control inputs* $u(t)$ *near the origin (see, e.g., (Sontag, 2009) for further details).* $\diamond$

The proposition below describes the necessary and sufficient conditions for developing differentiable CLFs for the control systems in the context of optical tweezers.

Proposition 1. *For the optical tweezer control system* (2.6)*, let* $W : \mathbb{R} \to \mathbb{R}_{\geq 0}$ *be a positive definite and continuous function. Then, a smooth function* $V : \mathbb{R} \to \mathbb{R}_{\geq 0}$ *is a differentiable CLF satisfying* (2.10) *if and only if*

$$W(x) - \zeta_0 \left| \frac{dV}{dx} \right| \leq 0, \ \ \textit{for all } x \in \mathbb{R}, \tag{2.11}$$

having $\zeta_0 := \frac{2\sqrt{3}}{9\beta_d} R\alpha_1$.

Proof. Given the function $W(\cdot)$, we define the mapping $G : \mathbb{R} \times \mathbb{R} \to \mathbb{R}$ by $(x, u) \mapsto \nabla V(x) \cdot f_{\text{twz}}(x,\, u,\, 0) + W(x)$, where $V(\cdot)$ is a differentiable function with derivative $\frac{dV(x)}{dx}$. Hence,

$$G(x, u) = \Big(\frac{dV}{dx}\Big) \cdot \frac{\varphi(x-u)}{\beta_d} P(x-u) + W(x), \tag{2.12}$$

where $P(x-u) := \alpha_3(x-u)^3 - \alpha_1(x-u)$ and $W(x)$ is a positive definite, continuous function. From (2.10), it follows that $V(\cdot)$ is a differentiable CLF for the unperturbed optical tweezer system if and only if

$$\min_{|u| \leq \sigma(|x|)} G(x, u) \leq 0 \ \text{ for all } x \in \mathbb{R}. \tag{2.13}$$

where $\sigma : \mathbb{R}_{\geq 0} \to \mathbb{R}_{\geq 0}$ is a nondecreasing function. For an arbitrary $x \in \mathbb{R}$, we define the mapping $H : \mathbb{R} \to \mathbb{R}$ by $u \mapsto G(x, u)$. Given the compact interval $\mathcal{I}_x := \big[-\sigma(|x|),\, \sigma(|x|)\big]$, the inequality in (2.13) holds if and only if

$$\min_{u\in\mathcal{I}_x} H(u) \leq 0 \text{ for all } x \in \mathbb{R}. \tag{2.14}$$

Since $H(u)$ is continuous, it achieves its global minimum on the compact interval $\mathcal{I}_x$ for each $x \in \mathbb{R}$. The critical points of $H(\cdot)$, where $\frac{dH}{du} = 0$, are given by $u_1^* = x - \left(\frac{\alpha_1}{3\alpha_3}\right)^{0.5}$ and $u_2^* = x + \left(\frac{\alpha_1}{3\alpha_3}\right)^{0.5}$, for which we have

$$H(u_{1,2}^*) = W(x) \pm \underbrace{\frac{2\sqrt{3}}{9\beta_d} R\alpha_1}_{\zeta_0} \frac{dV}{dx}. \tag{2.15}$$

Considering the boundary points of the interval $\mathcal{I}_x$, specifically $u_l = -\sigma(|x|)$ and $u_r = \sigma(|x|)$, we define $\kappa_r(x) := \frac{\varphi(x-u_r)}{\beta_d} P(x-u_r)$ and $\kappa_l(x) := \frac{\varphi(x-u_l)}{\beta_d} P(x-u_l)$. Therefore, we achieve

$$\min_{u\in\mathcal{I}_x} H(u) = W(x) + \min\Big\{ \pm \zeta_0 \frac{dV}{dx}, \kappa_r(x)\frac{dV}{dx}, \kappa_l(x)\frac{dV}{dx} \Big\}. \tag{2.16}$$

Subsequently, we can conclude

$$\min_{u\in\mathcal{I}_x} H(u) \leq W(x) - \zeta_0 \left| \frac{dV}{dx} \right|. \tag{2.17}$$

Finally, the proof of the proposition 1 is obtained by substituting (2.17) into Inequality (2.14). □

Remark 2. *As shown in Proposition 1, the physical parameters of the optical tweezer—such as the trapping radius, viscous damping factor of the environment, and trap stiffness coefficients—directly appear in the condition specified by* (2.11). ◇

Proposition 1 enables the construction of a range of smooth CLFs for the optical tweezer's non-affine-in-control nonlinear system. For example, the pair

$$W(x) = |x|,\ V(x) = \frac{1}{2\zeta} x^2, \tag{2.18}$$

where ζ is a positive constant with $0 < \zeta \leq \zeta_0$, satisfying the condition in Proposition 1. Therefore, $V_1(\cdot)$ qualifies as a smooth CLF for the optical tweezer control system. In some cases, directly controlling the decay rate of CLFs is desirable (see, e.g., (Tang and Daoutidis, 2019)). The following corollary, derived directly from Proposition 1, addresses this need for controlling the decay rate of CLFs.

Corollary 1. *Consider Proposition 1 and let*

$$\begin{aligned} W(x) &= \frac{1}{\zeta}\gamma(x)V(x), \\ V(x) &= V_0\Big\{ \exp\Big(\int_0^x \frac{\gamma(s)}{\zeta}\, ds\Big) - 1\Big\}, \end{aligned} \tag{2.19}$$

where $\gamma : \mathbb{R} \to \mathbb{R}_{\geq 0}$ is any continuous function with $\gamma(x) > 0$ for all $x \in \mathbb{R}\backslash\{0\}$ and $\gamma(0) \geq 0$. Additionally, V_0 is an arbitrary positive constant, and ζ is a positive constant with $0 < \zeta \leq \zeta_0$. Then $V(\cdot)$ is a smooth CLF for the optical tweezer.

As specific cases of Corollary 1, if $\gamma_1(x) = |x|$ and $\gamma_2(x) = \gamma_0$ where $\gamma_0 > 0$ is a positive constant, then

$$\begin{aligned} V_1(x) &= V_0\Big\{ \exp\big(\frac{x^2}{2\zeta}\big) - 1\Big\}, \text{ and} \\ V_2(x) &= V_0\Big\{ \exp\big(\frac{\gamma_0\, x}{\zeta}\big) - 1\Big\}. \end{aligned} \tag{2.20}$$

Therefore, V_1 and V_2 serve as smooth CLFs for the optical tweezer control system corresponding to $\gamma_1(\cdot)$ and $\gamma_2(\cdot)$, respectively.

2.5.2 CLF-based Robust Stabilizing Feedback

Once a smooth CLF is identified for the unperturbed optical tweezer system without disturbance input, the feedback input $u = k^*(x)$ can be determined to satisfy the steepest descent condition below.

$$k^*(x) := \underset{|u|\leq\sigma\left(|x|\right)}{\operatorname{argmin}} \; W(x) + \nabla V(x) \cdot f_{\text{twz}}(x,\, u,\, 0), \tag{2.21}$$

where the corresponding control law is a globally asymptotically stabilizing (GAS) feedback feedback for the perturbed optical tweezer system (2.9), accounting for sensor measurement errors and external disturbances, as established in (Sontag, 2009, Theorem 7).

Proposition 2, which leverages the proof of Proposition 1, eliminates the need to use an optimization algorithm to determine the steepest descent feedback law in (2.21).

Proposition 2. *Let $V(\cdot)$ be a differentiable CLF for the non-affine-in-control optical tweezer system given by* (2.6)*. Then, the steepest descent feedback control input satisfying* (2.21) *can be derived from*

$$k^*(x) = \underset{u\in\{x\pm(\frac{\alpha_1}{3\alpha_3})^{0.5},\pm\sigma(|x|)\}}{argmin} \; W(x) + \nabla V(x) \cdot f_{twz}(x, u, 0). \tag{2.22}$$

Proof. The proof follows directly from that of Proposition 1. Take into account any arbitrary position $x \in \mathbb{R}$. Hence, the feedback input u^* that minimizes $G(x, u)$ in (2.12) over the compact interval $\mathcal{I}_x = \big[-\sigma(|x|),\, \sigma(|x|)\big]$ is either one of the critical points $x \pm \left(\frac{\alpha_1}{3\alpha_3}\right)^{0.5}$ or one of the boundary points $\pm\sigma(|x|)$. □

Remark 3. *The unique structure of the non-affine-in-control optical tweezer nonlinear system obviates the need of solving the NLP given in* (2.22)*, which is a computationally intensive optimization scheme. Indeed, we can utilize Proposition 2 to determine the robust stabilizing feedback control $k^*(x)$ by evaluating only four values at each bead position.* ◇

2.5.3 Simulation Studies

In this section, we present numerical simulations that illustrate the effectiveness of the proposed control framework subjecting to external disturbances. The simulation parameters

are taken from (Ranaweera et al., 2003; Ranaweera and Bamieh, 2005) and are listed in Table 2.1. A particle held in the harmonic Gaussian beam of optical tweezer experiences an external random thermal Langevin force $F_e(t)$, modeled as external disturbances in the trap system dynamics, given in the equation (2.7). This force has a mean value of zero, $\langle F_e(t) \rangle = 0$, unit load impedance, and the constant power spectrum density (PSD) of $4\beta k_B T$, where k_B represents the Boltzmann's constant and T denotes the absolute temperature (Gittes and Schmidt, 1998). For the spherical bead of interest with radius $r_p = 1\,\mu$m, the PSD is approximately $1.6 \times 10^{-4}\,\mu\text{m}^2$ at room temperature.

We begin by modeling a globally asymptotically stabilizing (GAS) control law as proposed by Bamieh and colleagues (Ranaweera et al., 2003; Ranaweera and Bamieh, 2005). The very control law is derived by approximating the trapping force using a hyperbolic tangent function and reads as

$$k(x) = x - \omega \tanh\left(\frac{p}{\lambda \beta_d} x\right), \tag{2.23}$$

with $p = 10$, $\lambda = 5$, and $\omega = 0.3893\,\mu$m.

Figure 2.2 illustrates the time profile of the position of the bead, starting from $x(0) = 1\,\mu$m, under the control law given in equation (2.23). The inner plot shows the time profile of the optical trap effective stiffness. We can observe that both the control input x_T and the trap effective stiffness $\left|\frac{dF_t}{dx}\right|$ are subject to significant oscillations while stabilizing the postion of the bead. Additionally, sharp variations in the control input and trap effective stiffness profiles, occurring around $t \approx 3.9\,$ms, poses another noticeable challenge for effective control of the optical tweezer system. Specifically, an oscillatory relative position of the bead, x_r, about the origin drives subsequent oscillations in the effective stiffness and around $\frac{\alpha_1}{\beta_d}$, negatively impacting system stability. These oscillations in trap stiffness align with the behavior shown in the left plot of Figure 2.1, where oscillations in the bead's relative position around the origin correspond to fluctuations in stiffness near $\frac{\alpha_1}{\beta_d}$.

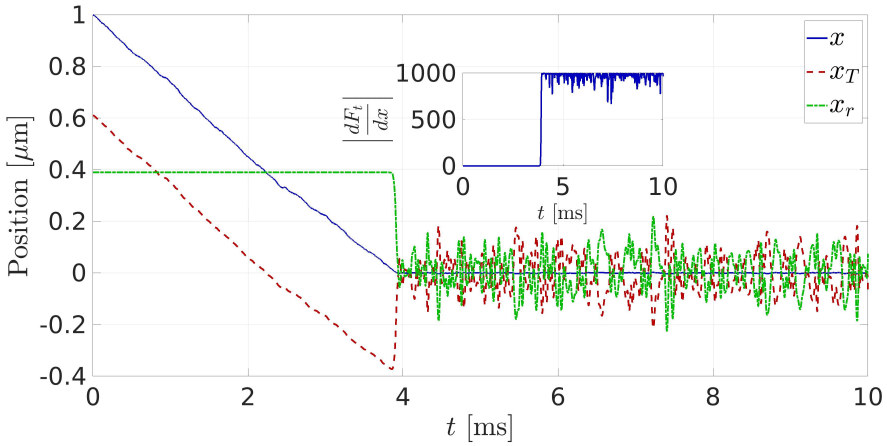

Figure 2.2: The position of the bead, initially located at $x(0) = 1\,\mu$m, is stabilized using the optical tweezer trap model under the GAS control law provided by (Ranaweera et al., 2003). The bead is under the external random thermal Langevin force with zero mean and a PSD with the approximate value of $1.6 \times 10^{-4}\,\mu\text{m}^2$. The inner plot demonstrates the time profile of the trap effective stiffness.

In the second set of numerical simulations, we modeled $\zeta = \zeta_0$, using the CLF pair $V(x)$ and $W(x)$ defined in (2.19). The optical trap effective stiffness is constrained by setting $\kappa_0 = \alpha_1$, resulting in $\sigma_T(|x|) = |x|$. Then, The stabilizing control input is generated by solving the NLP provided in equation (2.21), which requires no knowledge of external disturbances by setting $F_e = 0$.

Figure 2.3 illustrates the time profile of the bead position, starting from $x(0) = 1\,\mu$m, under the control law given by equation (2.21) with the CLF pair in equation (2.19) and having $\zeta = \zeta_0$. The inner plot shows the time profile of the optical trap effective stiffness. As seen in both plots, the commanded control input x_T and the trap effective stiffness $\left|\frac{dF_t}{dx}\right|$ exhibit minimal oscillations while effectively driving the bead position to a very small neighborhood around the origin. Notably, the time profile of the trap effective stiffness remains smoother than what it experiences in the GAS control law, a clear finding when comparing Figure 2.3 with 2.2.

From a control system bandwidth perspective, the proposed CLF-based control algorithm outperforms the ad-hoc controller in (2.23). As Sehgal *et al.* (Sehgal et al., 2009) noted,

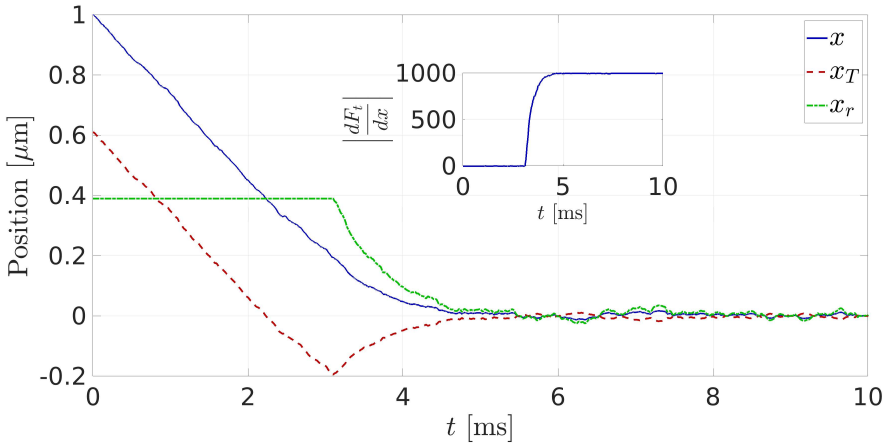

Figure 2.3: Stabilization of the bead position, starting from $x(0) = 1\,\mu$m, is achieved using the optical tweezer trap model under the proposed control law which we poroposed. The inner plot demonstrates the time profile of the effective stiffness of the trap. The bead is under the external random thermal Langevin force with zero mean and a PSD with the approximate value of $1.6 \times 10^{-4}\,\mu\text{m}^2$.

controlling the bead's position encounters significant limitations in bandwidth under the high-frequency force of optical tweezers.

2.6 Conclusion

This chapter introduced a Control Lyapunov Function (CLF)-based framework for robustly stabilizing a spherical particle within an optical tweezer system, targeting the core challenges of precise positioning and control. Through a CLF-based approach, we formulated a nonlinear optimization-based control strategy that balances stabilizing control forces with external disturbances. The resulting Nonlinear Programming (NLP) model offers robust feedback control inputs that stabilize the particle, even when initially positioned far from the laser beam, while compensating for thermal fluctuations.

A key feature of this framework is its focus on thermal effects—critical in optical trapping—where high laser power, though advantageous for swift manipulation, risks unwanted heating that can damage biological samples. By carefully defining force ranges, trap stiffness,

and other trap parameters, the control model ensures particle confinement within the optical trap while mitigating thermal stress. Numerical simulations confirm the robustness of this approach, showing its capacity to stabilize the particle against stochastic thermal forces. The model's constraints on trap stiffness effectively reduce oscillations and prevent power levels that might induce heating, thus protecting sensitive biomolecules.

This CLF-based framework advances control at the microscale and lays the groundwork for manipulating nanoscale biomolecules such as DNA, RNA, and proteins in future experiments—an effort further explored in Chapter 3 with a focus on manipulating nanoscale biomolecules such as DNA. Moving forward, developing refined control algorithms with temperature-regulation mechanisms will be essential to enhance trapping performance while minimizing thermal risks. This expansion could enable new applications in molecular biology, allowing precise, non-invasive manipulation of biomolecules under increasingly complex experimental conditions.

CHAPTER 3

CONTROL CHETAEV FUNCTION (CCF) FRAMEWORK FOR PROTEIN DENATURATION

3.1 Introduction

This chapter presents a control chetaev function (CCF)-based control framework to achieve controlled unfolding of a DNA using optical tweezers, with a focus on ensuring system instability to promote denaturation. Beginning with an overview of the force field model for optically trapped DNA in 3.2, we derive the governing equations, including trapping forces, the worm-like chain (WLC) model, Langevin forces, and viscous drag. Then, we examine the non-affine and the corresponding affine-in-control system dynamics in 3.2.1 and 3.2.2 to explore proper control approaches. Subsequently, we introduce CCFs as a foundation for designing closed-loop control inputs based on Chetaev's necessary and sufficient conditions, achieving controlled system instability for protein unfolding in 3.3. Additionally, in 3.4, we review universal control laws for instability as formulated by (Efimov et al., 2014), providing a structured approach for implementing unbounded and norm-bounded control inputs. Finally, Simulation studies, in 3.5, employ the Euler–Maruyama algorithm to numerically validate the control approach under thermal conditions and different sampling times.

3.2 Force Field Model

In this section, we outline the equation of motion that governs optically tapped polymers under the influence of potential forces, covering the non-affine and corresponding affine-in-control system dynamics. With respect to the force profile shown in Figure 3.1, the WLC force combined with thermal fluctuation attempt to move the particle out of the trap, while the trapping force draws it back towards the laser focus, maintaining a dynamic equilibrium.

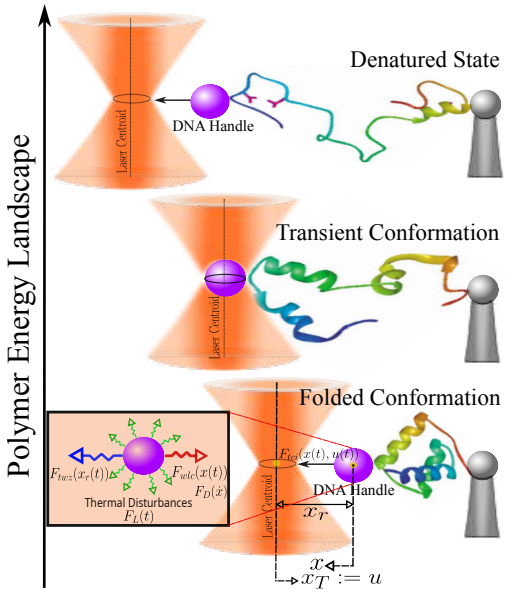

Figure 3.1: Schematic of the ensemble system of DNA and its trapping handle in the propagation of optical tweezer's harmonic Gaussian beam.

Therefore, the motion of an optically trapped DNA molecule through a Brownian trapping handle (a bead experiencing thermal disturbances modeled as Brownian motion) of mass m

$$m\ddot{x} = F_{twz}(x_r) - F_{wlc}(x) + F_L(t) - F_D(\dot{x}) + F_E(t) \tag{3.1}$$

where, $F_{twz}(.)$, $F_{wlc}(.)$, $F_L(.)$, $F_D(.)$, and $F_E(.)$ denote the trapping force, worm-like chain (WLC) force, Langevin force, viscous drag, and other external disturbances, respectively. The lateral bead displacement is determined by the bead position x and the laser focus position x_T, given as $x_r := x - x_T$.

The trapping force behaves as a nonlinear restoring spring and reads as

$$F_{twz}(x_r) = \phi(x_r)(\alpha_3 {x_r}^3 - \alpha_1 x_r), \tag{3.2}$$

with the maximum restoring force occuring at $|x_r| = R_{\max} = 0.3893\,\mu$m and the optical tweezer cut off R setting at $0.675\mu m$, which introduces the following trap saturation

$$\phi(x_r) = \begin{cases} 1 & \text{for } |x_r| < R \\ 0 & \text{otherwise.} \end{cases} \tag{3.3}$$

For the model parameters refer to Table 3.1. The trap force spring constants, α_1 and α_3, are derived from the observations of Simmons et al (Simmons et al., 1996) and taken from (Ranaweera et al., 2003), (Ranaweera and Bamieh, 2005), and (Golgoon et al., 2024). The WLC model is expressed as

$$F_{wlc} = \frac{k_B T}{L_p} \left[\frac{1}{4\left(1 - \frac{x}{L}\right)^2} - \frac{1}{4} + \frac{x}{L} \right]. \tag{3.4}$$

The WLC parameters are obtained from (Bustamante et al., 2020) (refer to Table 3.1). Specifically, l_p and L, representing the persistence and contour length of the DNA respectively, are derived from a nonlinear least-squares fit by Bustamante (Bustamante et al., 1994), through Figure 3.2.

The thermal noise, $F_L(t)$, is modeled as a random signal

$$F_L(t) = \sqrt{2S}\, W(t), \tag{3.5}$$

where $W(t)$ represents white noise and $2S$ the noise intensity. The formulation is due to the following properties: $\langle F_L(t) \rangle = 0$, $\langle F_L(t) x(t) \rangle = 0$, and $\langle F_L(t) F_L(t+\tau) \rangle = 2S\delta(\tau)$.

The viscous drag, $F_D(\dot{x})$, can be represented as

$$F_D(t) = \beta \dot{x}, \tag{3.6}$$

where the friction coefficient (β) is determined for a bead of radius r_p by the Stokes' law as $\beta = 6\pi\eta r_P$, with a fluid viscosity η.

By simplifying equation 3.1 under the condition that the setup is not influenced by any other external potential $F_E(t)$, and considering that $\phi(x_r)$ remains constant at 1 due to the

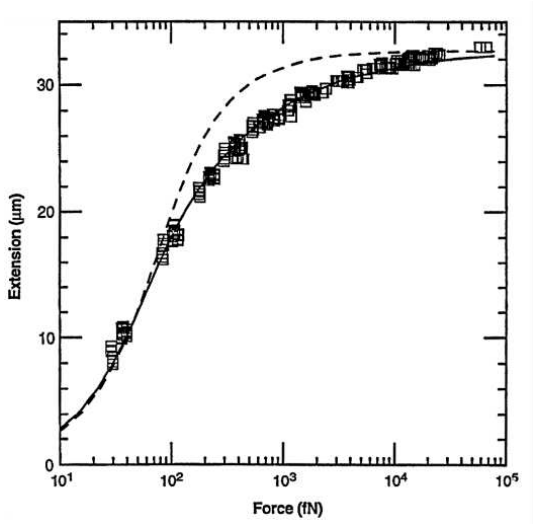

Figure 3.2: The force-extension profile through (Bustamante et al., 1994), where squares represent experimental force-extension data, and the solid line denotes a fit for the entropic force required to extend a worm-like polymer. Additionally, dashed curve represents the freely-jointed chain (FJC) model with the contour length of $32.7\mu m$ and the segment length of $100nm$ chosen to fit the small-force data.

persistence length being significantly smaller than the optical tweezer cutoff $l_P << r_P$, one can combine equations 3.2, 3.4, 3.5, and 3.6 to arrive at

$$m\ddot{x} = \alpha_3 {x_r}^3 - \alpha_1 x_r - \frac{k_B T}{L_p}\left[\frac{1}{4\left(1-\frac{x}{L}\right)^2} - \frac{1}{4} + \frac{x}{L}\right] - \sqrt{2S}\,W(t) - \beta\dot{x}. \tag{3.7}$$

3.2.1 Non-Affine-in-Control Dynamics

The system dynamics follows an overdamped Langevin equation and can be obtained from equation 3.7. Given the low Reynolds number—attributable to the slow motion of the handle in a viscous medium under a harmonic trapping potential—the mass of the bead becomes negligible. Therefore, the dynamics is governed by the Non-Affine-in-Control system

$$\dot{x} = \frac{1}{\beta}[F_{TWZ-DNA}(x(t), u(t))] - \xi(t), \tag{3.8}$$

where , $x \in \mathbb{R}$, $u \in \mathbb{U}$, and $\xi \in \mathbb{D}$. The continuous function $F_{TWZ-DNA}(x(t), u(t))$ maps $F_{TWZ-DNA} : \mathbb{R} \times \mathbb{U} \to \mathbb{R}$ and stands for the trap-chain interaction force with the definition $F_{TWZ-DNA}(x(t), u(t)) := F_{twz}(x_r(t)) - F_{wlc}(x(t))$. The control input u can be any measurable locally bounded signal $u(\cdot) : [0, \infty) \to \mathbb{U}$, here is considered to be the laser focus as $u := x_T$.

The thermal noise ($\xi(t)$) is determined through equation 3.5 and by the relation between the diffusion coefficient (D) and the dissipation constant (β) according to the fluctuation-dissipation theorem, $D = \frac{k_B T}{\beta}$, which leads to $\xi(t) = \sqrt{2D}\, W(t)$. Therefore, through equations 3.7 and 3.8, we can obtain

$$\begin{aligned}\dot{x} = \frac{1}{\beta}\left[\alpha_3(x-u)^3 - \alpha_1(x-u) - \frac{k_B T}{L_p}\left(\frac{1}{4\left(1-\frac{x}{L}\right)^2} - \frac{1}{4} + \frac{x}{L}\right)\right] \\ - \sqrt{2D}\, W(t).\end{aligned} \tag{3.9}$$

3.2.2 Affine-in-Control Dynamics

Due to the smoothness of vector field, $F_{TWZ-DNA}(x(t), u(t))$, and by linearization about the control input, the nonlinear non-affine system of interest can be modeled in an affine-in-control structure as

$$\dot{x} = f(x) + g(x)u + u(R(x,u)u), \tag{3.10}$$

where $f(x) = F_{TWZ-DNA}(x, 0)$ and $G(x) = \frac{\partial F_{TWZ-DNA}}{\partial u}(x, 0)$. Therefore, the exact linearization of the vector field with respect to input is

$$\begin{aligned}\dot{x} = \frac{1}{\beta}\left[\alpha_3 x^3 - \alpha_1 x - \frac{k_B T}{L_p}\left(\frac{1}{4\left(1-\frac{x}{L}\right)^2} - \frac{1}{4} + \frac{x}{L}\right)\right] \\ + \frac{1}{\beta}\left(\alpha_1 - 3\alpha_3 x^2\right) u - \frac{\alpha_3}{\beta}u^3 + \frac{3\alpha_3}{\beta}u^2 x - \sqrt{2D}\, W(t).\end{aligned} \tag{3.11}$$

By eliminating the higher order terms of u in equation 3.11, one can facilitate the use of universal feedback controls discussed in section 3.3. Therefore, the vector field can be expressed in an affine-like form of

$$\dot{x} = f(x) + g(x)u, \tag{3.12}$$

with $f(x) = \frac{1}{\beta}\left[\alpha_3 {x_r}^3 - \alpha_1 x_r - \frac{k_B T}{L_p}\left(\frac{1}{4\left(1-\frac{x}{L}\right)^2} - \frac{1}{4} + \frac{x}{L}\right)\right]$ and $g(x) = \frac{1}{\beta}\left(\alpha_1 - 3\alpha_3 x^2\right)$.

Table 3.1: Optical Tweezers simulation parameters.

(a) Particle term model parameters

Variable	Value	Variable	Value
m	5.5×10^{-10} mg	r_p	1 μm
α_3	22 pN/μm^3	α_1	10 pN/μm
R	0.674 μm	$R_{\max}$	0.3893 μm

(b) WLC term model parameters

Variable	Value	Variable	Value
l_p	53.4 ± 2.3 nm	L	32.8 ± 0.1 μm
$k_B T$	4.11×10^{-21} Nm	β	0.01 pNs/μm

3.3 Control Chetaev Function (CCF) Feedback Control Design

In this section, we develop a CCF-based feedback control framework aimed at destabilizing targeted system dynamics by leveraging the CCF properties. We first address the entropy constraints relevant to DNA unfolding within optical tweezers in 3.3.1, then define the objectives of the CCF-based control in 3.3.2, and finally explore the conditions under which the CCF satisfies the Small Control Property (SCP) in 3.3.3.

3.3.1 Trap Stifness

The entropy constraint for all $x \in \mathcal{V}^+$ follows:

$$k\,\text{Sign}\left(\frac{\partial V}{\partial x}\right) > \frac{f(x)}{|g(x)|} \tag{3.13}$$

which is due to $f(x) > -k|g(x)| - \text{Sign}\left(\frac{\partial V}{\partial x}\right)$.

$$TS^{\circ} = \zeta N L^{\circ 2} \tag{3.14}$$

The change rate of the entropy in the final phases of unfolding is related to the rate of collapse of the chain through equation 3.18, leading to a collapse time τ_c, where ζ, N, and S° respectively denote the monomer friction coefficient, the number of monomers in the chain, and the rate of change of entropy (see, (De Gennes, 1985)).

To unfold the DNA molecule with a bounded rate of change of entropy, denoted $\dot{S}$, we consider the biophysical properties of DNA modeled as a flexible coil. According to (De Gennes, 1985), the entropy change rate is given by $T\dot{S} \sim \eta \dot{x}^2 x$, indicating that the rate of entropy change increases with the DNA extension/unfolding rate.

We design a closed-loop control input to facilitate DNA unfolding while constraining $\dot{x}$. This is achieved by controlling the optical tweezer's trap position, thereby regulating the unfolding control input.

3.3.2 Problem Objective Through CCF-Based Control

Consider a norm-bounded control from $\mathcal{U}_k = \{u \in \mathbb{R} \mid |u| < k\}$, with some $k > 0$, and a smooth function $V : \mathcal{B}(\varepsilon_0) \to \mathbb{R}$ such that $V(0) = 0$, $\mathcal{V}^+ \cap \mathcal{B}(\varepsilon) \neq \emptyset$ for any $\varepsilon \in (0, \varepsilon_0]$, and that $\mathcal{V}^+ = \{x \in \mathcal{B}(\varepsilon_0) \mid V(x) > 0\}$. Then, V is a CCF with respect to the controls from $\mathcal{U}_k$ if for all $x \in \mathcal{V}^+$:

$$\sup_{u \in \mathcal{U}_k} \{a(x) + B(x)^T u\} > 0. \tag{3.15}$$

Considering that $a(x) = D^- V(x) f(x)$ and $B(x) = D^- V(x) g(x)$ are directional derivatives of the continuously differentiable function $V : \mathbb{R} \to \mathbb{R}_{\geq 0}$.

We take the trap position x_T as the control input u so that the position of the optical tweezer can be directly controlled. An acousto-optic deflector (AOD) actuates the trap focal

point position, x_T, and thus the bead's position is recorded by a digital camera (see (Shaevitz, 2006)).

3.3.3 CCF with the Small Control Property (SCP)

The CCF $V(x)$ for system 3.12 satisfies the Small Control Property (SCP) if for each $\varepsilon > 0$ $\exists \delta > 0$, such that if $x \in \mathcal{V}^+$ then $|x| < \delta$, i.e. if $x \in \mathcal{V}^+ \cap \{x : |x| < \delta\}$, then $\exists |u| < \varepsilon$ such that $a(x) + \mathcal{B}(x)u > 0$. The SCP property for a CCF holds if and only if

$$\lim_{|x| \to 0} \frac{a(x)}{|B(x)|} \geq 0 \tag{3.16}$$

for all $x \in \mathcal{V}^+$.

3.4 CCF-Based Feedback Control Laws for System Instability

This section reviews the universal control laws formulated by (Efimov et al., 2014), which provides necessary and sufficient conditions for achieving system instability through chetaev-based, destabilizing control strategies. These laws offer a framework that incorporate unbounded and norm-bounded control inputs, whichever best serves our interest.

3.4.1 Chetaev-Based Unbounded Control Law

If for the system 3.12 there exists a CCF $V : \mathcal{B}(\epsilon_0) \to \mathbb{R}$ with respect to controls from $\mathcal{U}_k$, then the control

$$u_{Efmv}(x) = \begin{cases} -[\frac{a(x) - \sqrt[p]{a(x)^p + B(x)^2 q}}{B(x)^2}] B(x) & \text{if } b \neq 0; \\ 0 & \text{if } b = 0 \end{cases} \tag{3.17}$$

is continuous for all $x \in \mathcal{V}^+$, having $2q \geq p > 1$, and $q > 1$, and ensures system instability in $\mathcal{B}(\epsilon_0)$ (see theorem 2 in (Efimov et al., 2014)).

3.4.2 Chetaev-Based Norm-Bounded Control Law

If for the system 3.12 there exists a CCF $V : \mathcal{B}(\epsilon_0) \to \mathbb{R}$ with respect to controls from $\mathcal{U}_k$, then the control

$$u_{Efmv}(x) = \begin{cases} -[\frac{a(x)-\sqrt{|a(x)|^p+B(x)^2q}}{B(x)^2(1+\sqrt[p]{1+k^{-p}B(x)^2q-p})}]B(x) & \text{if } b \neq 0; \\ 0 & \text{if } b = 0 \end{cases} \tag{3.18}$$

is continuous for all $x \in \mathcal{V}^+$, having $u(x) \in \mathcal{U}_k$, $2q \geq p > 1$, and $q > 1$, and ensures system instability in $\mathcal{B}(\epsilon_0)$ (see theorem 3 in (Efimov et al., 2014)).

3.5 Simulation Studies

We introduce the Euler–Maruyama algorithm, a numerical method for solving stochastic differential equations (SDEs) that include noise terms, such as those in Langevin dynamics 3.5.1. Building on the classic Euler method, the algorithm effectively captures stochastic influences, making it suitable for simulating DNA unfolding under thermal fluctuations. Here, Euler–Maruyama discretizes system dynamics to model DNA's response in an optical trap, facilitating the analysis of candidate Control Chetaev Functions (CCF) for the optical tweezer-DNA pair in 3.5.2.

3.5.1 Euler–Maruyama algorithm.

Euler–Maruyama algorithm is a numerical integration scheme specifically designed for solving stochastic differential equations (SDEs), which include random noise terms such as those present in Langevin dynamics. This method is an extension of the classical Euler method and provides a simple yet effective way to approximate solutions to SDEs by incorporating the effect of stochastic forces. Here, The Euler–Maruyama algorithm enables the simulation of the DNA unfolding process under thermal fluctuations by discretizing the system dynamics

over small time steps, allowing for accurate representation of random disturbances in the trapping environment. This approach is particularly suitable for systems where noise plays a significant role, such as in the molecular dynamics of optically trapped particles (see (Pesce et al., 2020)). The algorithm scheme is as follows:

$$\frac{x_{i+1} - x_i}{\Delta t} = \frac{1}{\beta}[F^{d,i}_{TWZ-DNA}] - \xi(t), \tag{3.19}$$

$$x_{i+1} = x_i + \frac{\Delta t}{\beta}[F^{d,i}_{TWZ-DNA}] - \sqrt{2D\Delta t}\, n_i. \tag{3.20}$$

where n_i is a Gaussian random variable with zero mean and unit variance. The time step Δt is significantly smaller than the characteristic time scales of the stochastic process, is chosen to be $1\mu sec$ in 3.5 (see (Volpe and Volpe, 2013) and (Pesce et al., 2020)).

3.5.2 Candidate CCF for Protein Unfolding Under Chetaev Conditions

The CCF $V(x) = x$ is a candidate CCF due to satisfying the necessary and sufficient conditions in section 3.3.2, outlined as follows: i) For all $0 < x < \sqrt{\frac{\alpha_1}{3\cdot\alpha_3}}$, $|B(x)| \neq 0$, which verifies it as a valid CCF; ii) The limit $\lim_{x\to 0} \frac{f_0(x)}{\left|\frac{1}{\beta_d}[\alpha_1 - 3\alpha_3 x^2]\right|} = 0$ holds, thereby confirming that the Small Control Property (SCP) is met, ensuring the system's responsiveness to small control inputs; iii) The inequality $k > \frac{a_3x^3 - a_1x - F_{\text{WLC}}(x)}{|-3a_3x^2 + a_1|}$ holds for all positive k and sufficiently small x, indicating that the control parameters support effective destabilization. Therefore, $V(x) = x$ serves as a suitable CCF candidate, allowing us to apply the universal control formulas in 3.3.2 to induce system instability according to the parameters listed in Table 3.1, and having $p = 2$, $q = 1.01$, and $k = 0.1\mu m$.

Figure. 3.4 demonstrates the effectiveness of the controller with a 1 ms sampling time, which is typical for optical tweezers experiments, through (Ranaweera et al., 2003).

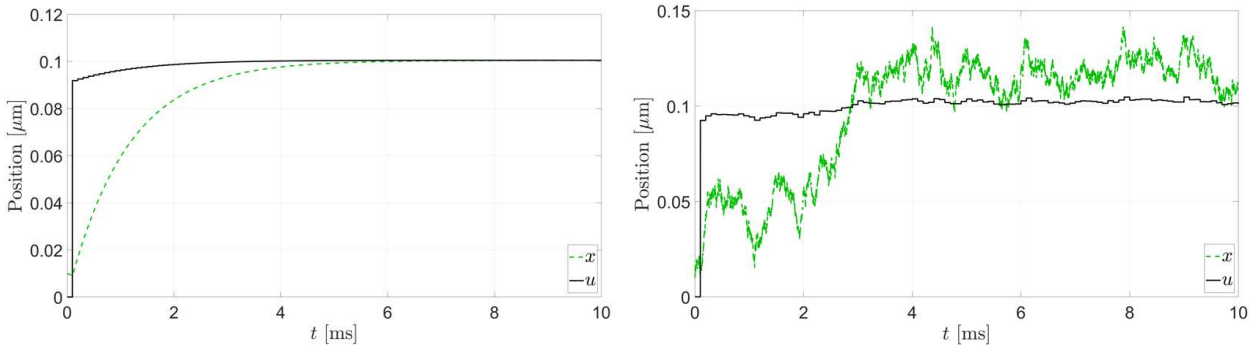

Figure 3.3: Simulation results with $T_{sampling} = 0.1ms$. The left picture is with no thermal noises and the right one is with the consideration of thermal disturbances.

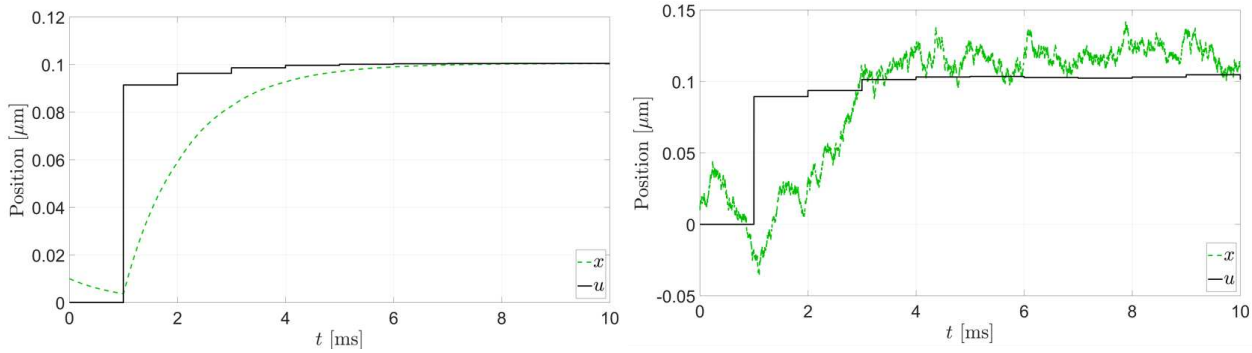

Figure 3.4: Simulation results with $T_{sampling} = 1ms$. The left picture is with no thermal noises and the right one is with the consideration of thermal disturbances.

3.6 Conclusion

This chapter introduced a Control Chetaev Function (CCF)-based framework for managing constrained, closed-loop unfolding of DNA molecules via optical tweezer systems. By leveraging the optical trapping potential and integrating key forces—including the trapping potential itself, worm-like chain (WLC) behavior, and thermal disturbances—the proposed model captures the intricate dynamics of optically trapped DNA. The candidate CCF for the optical tweezer-DNA pair was validated to meet small control properties, supporting precise manipulation within the practical limits. Leveraging linearization with respect to the control input, we designed controllers that achieve protein unfolding through system

instability, attained via closed-loop control inputs derived from the necessary and sufficient conditions of CCFs.

The findings illustrate that the proposed framework can effectively manage the delicate force interactions required for DNA unfolding, destabilizing the system in a controlled manner to promote denaturation. Simulations with thermal disturbances validated the robustness of this control approach, demonstrating its ability to achieve precise system behavior even under stochastic thermal influences. Ultimately, this control methodology offers a promising pathway for refined manipulation of biomolecular structures in optical tweezer experiments, where reliable control of single-molecule behavior is essential. Future work will include considering thermal and temperature effects for "safe" unfolding of DNA, which could further optimize control and reduce potential thermal stress on molecular structures during experimental manipulations. This enhances the potential for broader applications in molecular biology and biophysics.

CHAPTER 4

CONCLUSION

In this work, we developed an innovative control framework for the precise manipulation of biomolecules, with designing stable and destabilizing control laws for optical tweezers-driven manipulation tasks. It begins by establishing a stabilizing, Control Lyapunov Function (CLF)-based control input, effectively addressing the challenges posed by thermal fluctuations inherent in optical trapping of spherical beads. It improves the controller precision at the microscale and opens new possibilities for trapping and manipulating sensitive biomolecular structures like DNA and proteins.

Building on this foundation, we introduced a novel Control Chetaev Function (CCF)-based framework tailored for controlled instability, facilitating the unfolding of biomolecules and polypeptide chains. This approach leverages instability, enabling the exploration of transient molecular states otherwise obscured by traditional stabilization-focused methods. Our application of CCFs in optical tweezer control system represents a significant contribution, enabling DNA unfolding while minimizing thermal and mechanical stress. Simulation results confirmed that the proposed CCF-based control setup could reliably induce instability for protein denaturation, even under stochastic thermal noise, highlighting its potential for probing complex molecular dynamics.

To conclude, this thesis presents a comprehensive framework for both stable and unstable control of biomolecules with optical tweezers, advancing single-molecule studies in biophysics. The combination of CLF and CCF-based control methodologies equips researchers with powerful tools for precise manipulation at the nanoscale. This work lays a robust foundation for future advancements in the controlled manipulation of biomolecular structures. It fosters deeper insights into molecular mechanisms, critical to such fields as precision medicine and genetic engineering.

REFERENCES

Andersen, N. T. and J. Z. Chen (2024). Forced extension of a wormlike chain in the gibbs and helmholtz ensembles. *The Journal of Chemical Physics 160*(8).

Ashkin, A. (1980). Applications of laser radiation pressure. *Science 210*(4474), 1081–1088.

Ashkin, A., J. M. Dziedzic, J. E. Bjorkholm, and S. Chu (1986). Observation of a single-beam gradient force optical trap for dielectric particles. *Opt. lett. 11*(5), 288–290.

Braun, P., L. Grüne, and C. M. Kellett (2018). Complete instability of differential inclusions using lyapunov methods. In *2018 IEEE Conference on Decision and Control (CDC)*, pp. 718–724. IEEE.

Bugiel, M., A. Jannasch, and E. Schäffer (2017). Implementation and tuning of an optical tweezers force-clamp feedback system. *Optical Tweezers: Methods and Protocols*, 109–136.

Bustamante, C., L. Alexander, K. Maciuba, and C. M. Kaiser (2020). Single-molecule studies of protein folding with optical tweezers. *Annual review of biochemistry 89*(1), 443–470.

Bustamante, C., Y. R. Chemla, N. R. Forde, and D. Izhaky (2004). Mechanical processes in biochemistry. *Annual review of biochemistry 73*(1), 705–748.

Bustamante, C., J. F. Marko, E. D. Siggia, and S. Smith (1994). Entropic elasticity of λ-phage dna. *Science 265*(5178), 1599–1600.

Bustamante, C. J., Y. R. Chemla, S. Liu, and M. D. Wang (2021). Optical tweezers in single-molecule biophysics. *Nat. Rev. Methods Primers 1*(1), 25.

Camilli, F., L. Grüne, and F. Wirth (2008). Control Lyapunov functions and Zubov's method. *SIAM J. Contr. Optim. 47*(1), 301–326.

Chen, Z., Z. Cai, W. Liu, and Z. Yan (2022). Optical trapping and manipulation for single-particle spectroscopy and microscopy. *The Journal of Chemical Physics 157*(5).

Chi, W., X. Jiang, and Y. Zheng (2022). A linearization of centroidal dynamics for the model-predictive control of quadruped robots. In *2022 Int. Conf. Robot. Autom. (ICRA)*, pp. 4656–4663. IEEE.

da Fonseca, A. L., K. Diniz, P. B. Monteiro, L. B. Pires, G. T. Moura, M. Borges, R. S. Dutra, D. S. Ether Jr, N. B. Viana, and P. A. M. Neto (2024). Tailoring bistability in optical tweezers with vortex beams and spherical aberration. *Physical Review Research 6*(2), 023226.

De Gennes, P. (1985). Kinetics of collapse for a flexible coil. *Journal de Physique Lettres 46*(14), 639–642.

Efimov, D., W. Perruquetti, and M. Petreczky (2014). On necessary conditions of instability and design of destabilizing controls. In *53rd IEEE Conference on Decision and Control*, pp. 3915–3917. IEEE.

Fiasconaro, A. and F. Falo (2023). Elastic traits of the extensible discrete wormlike chain model. *Physical Review E 107*(2), 024501.

Furqon, R., Y.-J. Chen, M. Tanaka, K. Tanaka, and H. O. Wang (2016). An SOS-based control Lyapunov function design for polynomial fuzzy control of nonlinear systems. *IEEE Trans. Fuzzy Syst. 25*(4), 775–787.

Galloway, K., K. Sreenath, A. D. Ames, and J. W. Grizzle (2015). Torque saturation in bipedal robotic walking through control Lyapunov function-based quadratic programs. *IEEE Access 3*, 323–332.

Ghislain, L. P., N. A. Switz, and W. W. Webb (1994). Measurement of small forces using an optical trap. *Review of Scientific Instruments 65*(9), 2762–2768.

Gittes, F. and C. F. Schmidt (1998). Thermal noise limitations on micromechanical experiments. *Eur. Biophys. J. 27*, 75–81.

Golgoon, M., A. Mohammadi, and M. W. Spong (2024). A control lyapunov function-based approach for particle nanomanipulation via optical tweezers. In *2024 American Control Conference (ACC)*, pp. 2116–2121. IEEE.

Greenleaf, W. J., M. T. Woodside, E. A. Abbondanzieri, and S. M. Block (2005). Passive all-optical force clamp for high-resolution laser trapping. *Physical review letters 95*(20), 208102.

Grier, D. G. (2003). A revolution in optical manipulation. *nature 424*(6950), 810–816.

Hong, Z., H. Tang, Y. Xu, Z. Wu, and J. Li (2020). A new high-bandwidth nanopositioning tracking control method with input shaper and integral resonance controller. *Procedia CIRP 89*, 182–188.

Hyeon, C. and D. Thirumalai (2006). Kinetics of interior loop formation in semiflexible chains. *The Journal of chemical physics 124*(10).

Jahn, M., J. Buchner, T. Hugel, and M. Rief (2016). Folding and assembly of the large molecular machine hsp90 studied in single-molecule experiments. *Proceedings of the National Academy of Sciences 113*(5), 1232–1237.

Jones, P., O. Maragó, and G. Volpe (2015). *Optical tweezers*. Cambridge University Press Cambridge.

Kellermayer, M. S., S. B. Smith, H. L. Granzier, and C. Bustamante (1997). Folding-unfolding transitions in single titin molecules characterized with laser tweezers. *Science 276*(5315), 1112–1116.

Kratky, O. and G. Porod (1949). Röntgenuntersuchung gelöster fadenmoleküle. *Recueil des Travaux Chimiques des Pays-Bas 68*(12), 1106–1122.

Kubo, R., Y. Fujii, and H. Nakamura (2020). Control Lyapunov function design for trajectory tracking problems of wheeled mobile robot. *IFAC-PapersOnLine 53*(2), 6177–6182.

Lal, R. and S. A. John (1994). Biological applications of atomic force microscopy. *Am. J. Physiol.-Cell Physiol. 266*(1), C1–C21.

Ledyaev, Y. S. and E. D. Sontag (1999). A Lyapunov characterization of robust stabilization. *Nonlinear Anal. 37*(7), 813–840.

Lee, M. P. and M. J. Padgett (2012). Optical tweezers: A light touch. *Journal of Microscopy 248*(3), 219–222.

Li, L., S. S. Aphale, and L. Zhu (2021). High-bandwidth nanopositioning via active control of system resonance. *Frontiers of Mechanical Engineering 16*, 331–339.

Li, M., Y. Feng, and L. Liu (2023). Nanorobotics for investigating cell mechanics based on atomic force microscopy. In *Robot. Cell Manip. Charact.*, pp. 289–305. Elsevier.

Li, M., N. Xi, Y. Wang, and L. Liu (2020). Progress in nanorobotics for advancing biomedicine. *IEEE Trans. Biomed. Eng. 68*(1), 130–147.

Li, X. and C. C. Cheah (2017). Stochastic optical trapping and manipulation of a micro object with neural-network adaptation. *IEEE/ASME Trans. Mechatron. 22*(6), 2633–2642.

Li, X., C. C. Cheah, S. Hu, and D. Sun (2013). Dynamic trapping and manipulation of biological cells with optical tweezers. *Automatica 49*(6), 1614–1625.

Loeff, L., J. W. Kerssemakers, C. Joo, and C. Dekker (2021). Autostepfinder: A fast and automated step detection method for single-molecule analysis. *Patterns 2*(5).

Mack, A., M. Trias, and S. Mochrie (2009). Precision optical trapping via a programmable direct-digital-synthesis-based controller for acousto-optic deflectors. *Review of Scientific Instruments 80*(1).

Mohammadi, A. and M. W. Spong (2021). Integral line-of-sight path following control of magnetic helical microswimmers subject to step-out frequencies. *Automatica 128*, 109554.

Mohammadi, A. and M. W. Spong (2022a). Chetaev instability framework for kinetostatic compliance-based protein unfolding. *IEEE Contr. Syst. Lett. 6*, 2755–2760.

Mohammadi, A. and M. W. Spong (2022b). Quadratic optimization-based nonlinear control for protein conformation prediction. *IEEE Contr. Syst. Lett. 6*, 373–378.

Neuman, K. C. and A. Nagy (2008). Single-molecule force spectroscopy: optical tweezers, magnetic tweezers and atomic force microscopy. *Nature Methods 5*(6), 491–505.

Neupane, K., D. A. Foster, D. R. Dee, H. Yu, F. Wang, and M. T. Woodside (2016). Direct observation of transition paths during the folding of proteins and nucleic acids. *Biophysical Journal 110*(3), 517a.

Nieminen, T. A., V. L. Loke, A. B. Stilgoe, G. Knöner, A. M. Brańczyk, N. R. Heckenberg, and H. Rubinsztein-Dunlop (2007). Optical tweezers computational toolbox. *J. Opt. A: Pure Appl. Opt. 9*(8), S196.

Onal, C. D., O. Ozcan, and M. Sitti (2010). Automated 2-d nanoparticle manipulation using atomic force microscopy. *IEEE Trans. Nanotechnol. 10*(3), 472–481.

Oubellil, R., A. Voda, M. Boudaoud, and S. Régnier (2019). Mixed stepping/scanning mode control of stick-slip sem-integrated nano-robotic systems. *Sensors and Actuators A: Physical 285*, 258–268.

Pesce, G., P. H. Jones, O. M. Maragò, and G. Volpe (2020). Optical tweezers: theory and practice. *The European Physical Journal Plus 135*, 1–38.

Pfitzner, E., C. Wachauf, F. Kilchherr, B. Pelz, W. M. Shih, M. Rief, and H. Dietz (2013). Rigid dna beams for high-resolution single-molecule mechanics. *Angewandte Chemie International Edition 52*(30), 7766–7771.

Ranaweera, A. (2004). *Investigations with optical tweezers: construction, identification, and control*. University of California, Santa Barbara.

Ranaweera, A., K. Astrom, and B. Bamieh (2004). Lateral mean exit time of a spherical particle trapped in an optical tweezer. In *2004 43rd IEEE Conf. Dec. Contr. (CDC)*, pp. 4891–4896. IEEE.

Ranaweera, A. and B. Bamieh (2005). Modelling, identification, and control of a spherical particle trapped in an optical tweezer. *International Journal of Robust and Nonlinear Control: IFAC-Affiliated Journal 15*(16), 747–768.

Ranaweera, A., B. Bamieh, and A. R. Teel (2003). Nonlinear stabilization of a spherical particle trapped in an optical tweezer. In *42nd IEEE International Conference on Decision and Control (IEEE Cat. No. 03CH37475)*, Volume 4, pp. 3431–3436. IEEE.

Reed, A., G. O. Berger, S. Sankaranarayanan, and C. Heckman (2023). Verified path following using neural control Lyapunov functions. In *Conf. Robot Learn.*, pp. 1949–1958. PMLR.

Roychowdhury, S., T. Aggarwal, S. Salapaka, and M. V. Salapaka (2013). High bandwidth optical force clamp for investigation of molecular motor motion. *Applied Physics Letters 103*(15).

Roychowdhury, S., S. Bhaban, S. Salapaka, and M. Salapaka (2013). Design of a constant force clamp and estimation of molecular motor motion using modern control approach. *2013 American Control Conference*, 1525–1530.

Sehgal, H., T. Aggarwal, and M. V. Salapaka (2009). High bandwidth force estimation for optical tweezers. *Appl. Phys. Lett. 94*(15).

Shaevitz, J. W. (2006). A practical guide to optical trapping. *University of Washington 138*.

Shi, C., D. K. Luu, Q. Yang, J. Liu, J. Chen, C. Ru, S. Xie, J. Luo, J. Ge, and Y. Sun (2016). Recent advances in nanorobotic manipulation inside scanning electron microscopes. *Microsyst. Nanoeng. 2*(1), 1–16.

Simmons, R. M., J. T. Finer, S. Chu, and J. A. Spudich (1996). Quantitative measurements of force and displacement using an optical trap. *Biophysical journal 70*(4), 1813–1822.

Sontag, E. D. (2009). *Stability and Feedback Stabilization*, pp. 8616–8630. New York, NY: Springer New York.

Stigler, J., F. Ziegler, A. Gieseke, J. C. M. Gebhardt, and M. Rief (2011). The complex folding network of single calmodulin molecules. *Science 334*(6055), 512–516.

Tang, W. and P. Daoutidis (2019). A bilevel programming approach to the convergence analysis of control-lyapunov functions. *IEEE Trans. Automat. Contr. 64*(10), 4174–4179.

Taylor, A. J., V. D. Dorobantu, H. M. Le, Y. Yue, and A. D. Ames (2019). Episodic learning with control Lyapunov functions for uncertain robotic systems. In *2019 IEEE/RSJ Int. Conf. Intelli. Robot. Syst. (IROS)*, pp. 6878–6884. IEEE.

Tyson, C., C. McAndrew, P. Tuma, I. Pegg, and A. Sarkar (2015). Automated nonparametric method for detection of step-like features in biological data sets. *Cytometry Part A 87*(5), 393–404.

Volpe, G. and G. Volpe (2013). Simulation of a brownian particle in an optical trap. *American Journal of Physics 81*(3), 224–230.

Xie, H. and S. Régnier (2010). High-efficiency automated nanomanipulation with parallel imaging/manipulation force microscopy. *IEEE Trans. Nanotechnol. 11*(1), 21–33.

Yang, C. and K. Youcef-Toumi (2022). Decoupled tracking and damping control of piezo-actuated nanopositioner enabled by multimode charge sensing. *Mechanical Systems and Signal Processing 173*, 109046.

Yu, H., X. Liu, K. Neupane, A. N. Gupta, A. M. Brigley, A. Solanki, I. Sosova, and M. T. Woodside (2012). Direct observation of multiple misfolding pathways in a single prion protein molecule. *Proceedings of the National Academy of Sciences 109*(14), 5283–5288.

Zaltron, A., M. Merano, G. Mistura, C. Sada, and F. Seno (2020). Optical tweezers in single-molecule experiments. *The European Physical Journal Plus 135*(11), 896.

Zarrintaj, P., M. R. Saeb, F. J. Stadler, M. K. Yazdi, M. N. Nezhad, S. Mohebbi, F. Seidi, M. R. Ganjali, and M. Mozafari (2022). Human organs-on-chips: A review of the state-of-the-art, current prospects, and future challenges. *Adv. Biol. 6*(1), 2000526.

Zhang, X., L. W. Rogowski, and M. J. Kim (2019). 3D micromanipulation of particle swarm using a hexapole magnetic tweezer. In *2019 IEEE/RSJ Int. Conf. Intelli. Robot. Syst. (IROS)*, pp. 1581–1586. IEEE.

Zhang, X., L. W. Rogowski, and M. J. Kim (2020). Closed-loop control using high power hexapole magnetic tweezers for 3D micromanipulation. *J. Bionic Eng. 17*, 113–122.

Zhao, J., H. Hou, Q.-Y. Huang, X.-G. Zhong, and P.-S. Zheng (2022). Design of optical tweezers manipulation control system based on novel self-organizing fuzzy cerebellar model neural network. *Applied Sciences 12*(19), 9655.

BIOGRAPHICAL SKETCH

Melika Golgoon earned her BSc in Industrial Engineering with a concentration in Operations Research from K. N. Toosi University of Technology in 2022. Following her strong interest in designing optimization-based real-time control frameworks, Melika joined The University of Texas at Dallas in 2022 to pursue her master's degree in Systems Engineering and Management, with a concentration in optimization and control systems.

During her internship with Tesla Inc.'s production control team, she led the development of a real-time logistics system, achieving significant cost savings, 98% predictive accuracy, and a 40% process improvement. Melika's research interests focus on developing Lyapunov-based nonlinear control models for optical tweezer manipulation tasks, enhancing single-molecule manipulation in stable and unstable conditions. Her thesis advances nanorobotics by introducing Lyapunov-based feedback control frameworks for particle manipulation and protein unfolding tasks via optical tweezers.

CURRICULUM VITAE

Melika Golgoon

December 11, 2024

Educational History:

BS in Industrial Engineering , Concentration in Operations Research, K. N. Toosi University of Technology, 2018-2022
MS in Systems Engineering & Management, Concentration in Optimization & Control Systems, 2022-2024

Lyapunov-Based Nonlinear Control Strategies for Manipulation of Particles and Biomolecules Using Optical Tweezers
Master's Degree Thesis
Systems Engineering Department, University of Texas at Dallas
Advisor: Dr. Mark W. Spong

Publications:

Golgoon, Melika, Alireza Mohammadi, and Mark W. Spong. "A Control Lyapunov Function-Based Approach for Particle Nanomanipulation via Optical Tweezers." In 2024 American Control Conference (ACC), pp. 2116-2121. IEEE, 2024.

Golgoon, Melika, Alireza Mohammadi, and Mark W. Spong. "A Control Chetaev Framework for Optical Tweezer-Based Single-Molecule Unfolding of Protein Molecules." To be submitted.

Employment History:

Research
Graduate Research Assistant, Univeristy of Texas at Dallas, August 2022 – December 2023, June 2024 – December 2024

Industry
Industrial Engineer Intern, Tesla Inc., January 2024 – May 2024
Operations Research Analyst Intern, Secco Co., August 2021 – January 2022

Professional Recognitions and Honors:

Erik Jonsson School of Engineering and Computer Science Scholarship, University of Texas at Dallas, 2024
ORCGS Doctoral Fellowship, University of Central Florida, 2022
IE Wildcat Scholarship, University of Arizona, 2022
Doctoral Fellowship, Auburn University, 2022
Ranked top 3% among students of the Industrial Engineering Dept. in B.Sc., K. N. Toosi University of Technology, 2022

Ranked 1st in “Operations Research & Analytics” competition in B.Sc., K. N. Toosi University of Technology, 2021

Professional Service:

Reviewer
The IEEE Control Systems Society